CHEMISTRY
A EUROPEAN JOURNAL

DOI: 10.1002/chem.201000748

Simple Conjugated Polymers with On-Chain Phosphorescent Iridium(III) Complexes: Toward Ratiometric Chemodosimeters for Detecting Trace Amounts of Mercury(II)

Hui-Fang Shi, Shu-Juan Liu, Hui-Bin Sun, Wen-Juan Xu, Zhong-Fu An, Jian Chen, Shi Sun, Xiao-Mei Lu, Qiang Zhao,* and Wei Huang*[a]

Abstract: For the development of excellent optical probes for mercury(II), a series of simple conjugated polymers that contain phosphorescent iridium(III) complexes as receptors for mercury(II) were designed and synthesized. These conjugated polymers showed energy transfer from the polymer host to iridium(III) complex guest in both solution and the solid state. Unexpectedly, they can work as excellent polymer chemodosimeters for mercury(II) by utilizing the mercury(II)-induced decomposition of iridium(III) complex. They exhibit a pronounced optical signal change with switchable phosphorescence and fluorescence, even when the concentration of a solution of mercury(II) in THF was as low as 0.5 ppb. With the addition of mercury(II), the phosphorescent emission intensity of iridium(III) complexes was quenched completely. As the emission from polymer backbones increased, the emission wavelength was redshifted simultaneously, thereby realizing ratiometric detection. Excellent selectivity toward mercury(II) over other potentially interfering cations was also realized. In addition, an obvious emission color change of polymer solution from red to yellow-green was observed, thus realizing a "naked-eye" detection of mercury(II). More importantly, the solid films of these polymer chemodosimeters also exhibited high sensitivity and rapid response to mercury(II), thereby demonstrating the possibility of the fabrication of sensing devices with fast and convenient detection of mercury(II). The sensing mechanism was also investigated in detail. This is the first report on chemodosimeters based on conjugated polymers with phosphorescent iridium(III) complexes.

Keywords: chemodosimeters · host–guest systems · iridium · mercury · polymers

Introduction

Mercury is considered to be one of the most deleterious global pollutants.[1] It gives rise to serious health problems in the human body, even if its content is very low. For example, marine organisms can convert inorganic mercury into neurotoxic methylmercury, a potent neurotoxin that can easily enter the food chain and accumulate in the upper level of the food chain, particularly in the tissues of large edible fish and marine mammals.[2] Subsequently, the accumulation of mercury(II) and its conversion to the organic mercury compounds in the human body can lead to brain damage and serious cognitive and motion disorders[3] such as Minamata disease.[4] In 2004, the World Health Organization (WHO) established a guideline for drinking water quality, namely, that the concentration of mercury in water should be less than 1 mg L^{-1}.[5] Hence, the detection of trace amounts of mercury(II) is very important.

Traditional analytical techniques for mercury(II) quantification include atomic absorption spectroscopy, cold-vapor atomic fluorescence spectrometry, and gas chromatography. These methods, however, require not only complicated instrumentation but also a long measuring time. Therefore, it is urgent to develop new methods for monitoring mercury(II) with a low limit of detection, as well as rapid and facile detection. The use of fluorescent probes offers numer-

[a] H.-F. Shi, Dr. S.-J. Liu, H.-B. Sun, W.-J. Xu, Z.-F. An, J. Chen, S. Sun, X.-M. Lu, Dr. Q. Zhao, Prof. W. Huang
Key Laboratory for Organic Electronics & Information Displays (KLOEID)
and Institute of Advanced Materials (IAM)
Nanjing University of Posts & Telecommunications (NUPT)
9 Wenyuan Road, Nanjing 210046 (P.R. China)
Fax: (+86) 25-8586-6396
E-mail: iamqzhao@njupt.edu.cn
wei-huang@njupt.edu.cn

Supporting information for this article is available on the WWW under http://dx.doi.org/10.1002/chem.201000748.

ous advantages in terms of sensitivity, selectivity, response time, and low cost. More importantly, the fluorescent probes can be treated as one of the significant components in the signal processing and communication of a sensor network, which is a spatiotemporal sampling framework with a wireless communications infrastructure widely applied in environmental monitoring.

Recently, reaction-based chemical indicators, namely, chemodosimeters, have attracted increasing attention within the chemical sensory community. Chemodosimeters can be defined as those in which the visualized response is based on an irreversible or essentially irreversible reaction between the dosimeter molecule and analytes, which allows for selective and sensitive signaling.[6]

Up to now, most reported fluorescent probes, including chemodosimeters, have been based on pure organic fluorophores. In comparison with pure organic fluorophores, phosphorescent heavy-metal complexes exhibit advantageous photophysical properties such as relatively long emission lifetimes and significant Stokes shifts for easy separation of excitation and emission.[7] Among the phosphorescent complexes, iridium(III) complexes have been considered to be one of the best phosphorescent materials due to their intense phosphorescence at room temperature, significantly shorter emission lifetime compared with other heavy-metal complexes,[8] and tunable emission colors in the entire visible region by modifying the structure of the ligand. Hence, they have been applied successfully in organic light-emitting devices (OLEDs)[9] and luminescent biological labeling reagents.[10] Up to now, the use of iridium(III) complexes as chemosensors has also attracted considerable attention due to their sensitive emission properties in response to the changes in the local environment and significant single-photon excitation in the visible range.[11] Furthermore, many iridium(III)-complex-based chemosensors for cations, anions, and biomolecules have been reported.[12] However, as far as we know, the design of these iridium(III)-complex-based chemosensors is still limited to small molecules. As a class of promising light-emitting materials, the application of conjugated polymers that contain phosphorescent iridium(III) complexes as chemosensors has not yet been reported.

Conjugated polymer-based fluorescent chemosensors have been successfully utilized in the detection of a variety of analytes, including ions,[13] explosives,[14] and biomolecules.[15] In comparison with small molecular fluorophores, conjugated polymers, as delocalized π-electronic "molecular wires," allow for more rapid and efficient intrachain and interchain exciton migrations, and consequently amplified signal outputs can be realized.[16]

Hence, considering the importance of detection for mercury(II) and the advantages of phosphorescent iridium(III) complexes and conjugated polymers as probes, we introduced red-emitting phosphorescent iridium(III) complexes (as energy guests and receptors for mercury(II)) into polyfluorene backbones (as energy hosts) and realized a class of excellent conjugated polymer-based chemodosimeters for mercury(II).

Results and Discussion

Synthesis and characterization: The synthetic routes of the iridium(III) complex monomer ($\mathbf{M_3}$) and model compound (**4**) are shown in Scheme 1. The monomer $\mathbf{M_3}$ was synthesized from the corresponding 1,3-bis(4-bromophenyl)propane-1,3-dione (**3**) and iridium chlorido-bridged dimers (**2**). The copolymers were prepared through Suzuki polycondensation reaction from fluorene monomers ($\mathbf{M_1}$ and $\mathbf{M_2}$) and iridium(III) complex monomer ($\mathbf{M_3}$) shown in Scheme 2. The feed ratios of iridium(III) complex in the polycondensation reaction were 0, 2, 12, and 16 mol%, and the corresponding polymers were named poly(9,9-dioctylfluorene)

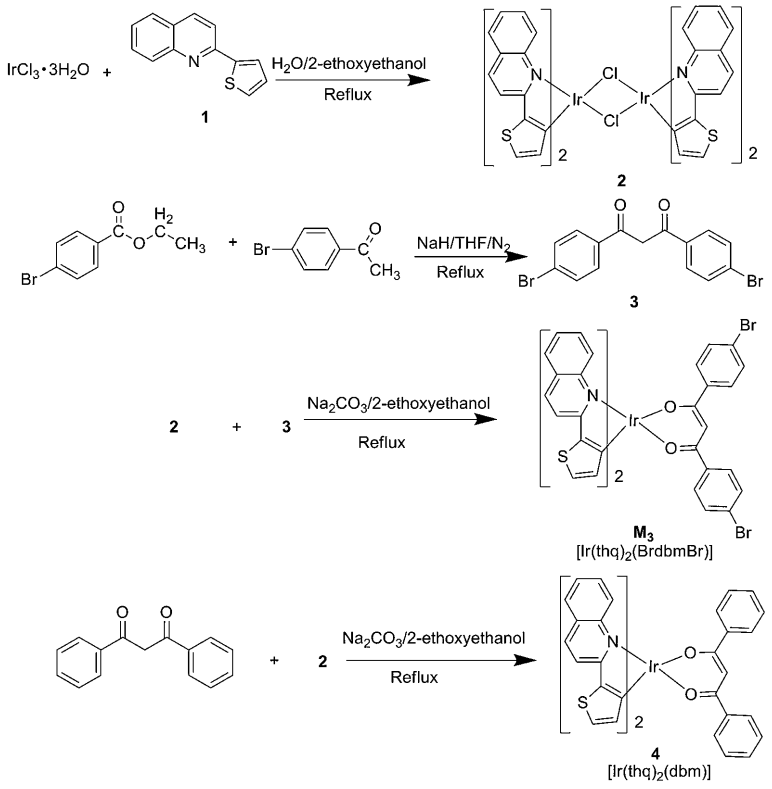

Scheme 1. Synthetic routes of iridium(III) complex monomer $\mathbf{M_3}$ and model iridium(III) complex **4**.

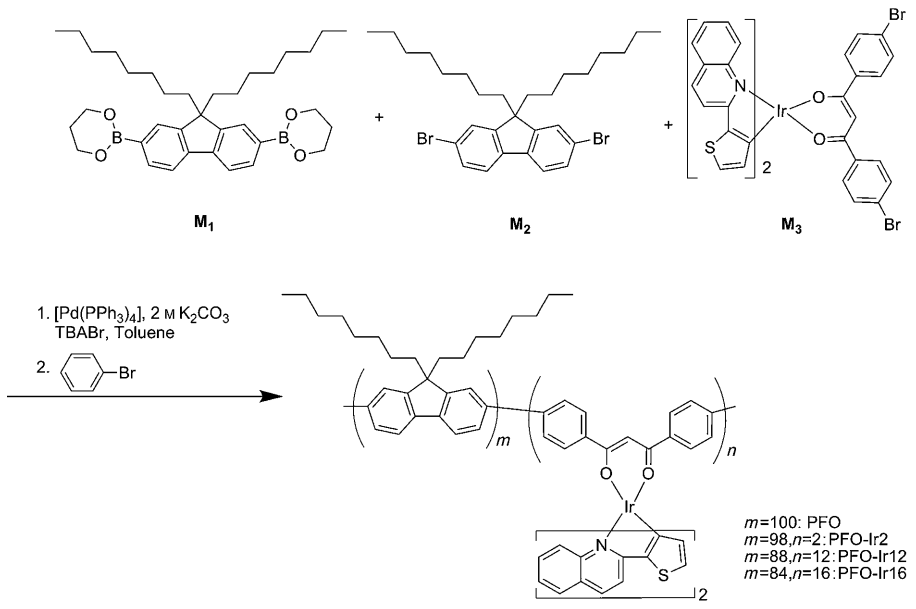

Scheme 2. Synthetic routes of conjugated polymers.

(PFO), PFO-Ir2, PFO-Ir12, and PFO-Ir16, respectively. Iridium(III) complex contents in the copolymers were estimated by the ^{1}H NMR spectra as shown in Table 1.[17] It was found that the actual contents of iridium(III) complexes in the conjugated polymers were lower than those in the feed ratios, which can be attributed to the difference of reactive activity and/or steric hindrance of iridium(III) complex units. The weight-average molecular weights (M_w) of these polymers estimated by GPC ranged from 9900 to 12100 with a polydispersity index (PDI) of 1.52–1.81, which are consistent with a Suzuki polycondensation reaction.[18]

Table 1. Molecular weight, polydispersity index, and composition of the polymers.

Polymers	M_w[a]	PDI	Complex content [mol%]	
			feed ratio	actual content[b]
PFO	12100	1.81	0	–
PFO-Ir2	10100	1.53	2	1.98
PFO-Ir12	10200	1.69	12	8.33
PFO-Ir16	9900	1.52	16	9.10

[a] Weight-average molecular weight (M_w) was estimated by GPC in THF by using a calibration curve of polystyrene standards. [b] Estimated from the ^{1}H NMR spectra.[17a]

Photophysical properties: The absorption and emission properties of polymers in both solution and film were studied (Figure 1) and are summarized in Table 2. Figure 1a shows the absorption and photoluminescence (PL) spectra of solutions of polymer PFO, PFO-Ir2, PFO-Ir12, and PFO-Ir16 in THF. An intense absorption band at around 380 nm is observed for all polymers. This band is assigned to the absorption of π–π* transitions of PFO backbones. In addition, a weak absorption band is observed in the range of 400–550 nm for the polymers that contain iridium(III) complexes. Its intensity enhances with an increase in iridium(III) complex content. This visible absorption band is attributed to the metal-to-ligand charge-transfer (MLCT) transitions of the iridium(III) complex units.[17a] The absorption spectra of these polymers in films are shown in Figure 1b, which are similar to those in solutions.

In the Förster energy-transfer mechanism,[19] the dipole–dipole interaction results in efficient transfer of the singlet-excited-state energy from the host to the guest. The efficiency of Förster energy transfer depends on the spectral overlap between the emission spectrum of host and the absorption spectrum of

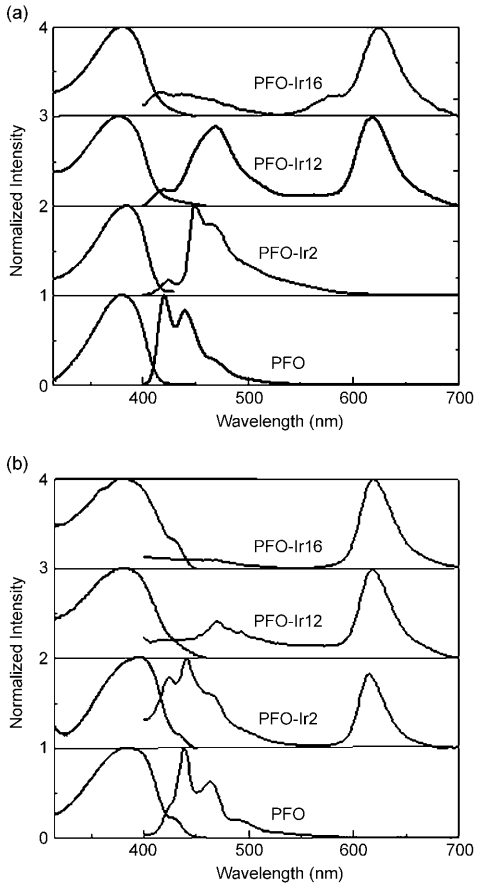

Figure 1. Absorption and PL spectra of polymers in a) solutions in THF (20 μM) and b) films (λ_{ex} = 360 nm).

guest.[20] Due to the good spectral overlap between the PL spectrum of the host PFO and the absorption spectrum of

Table 2. Photophysical properties of the conjugated polymers.

Polymers	UV (λ_{max} [nm])		PL (λ_{max} [nm])	
	solvent	film	solvent	film
PFO	380	382	422, 441	439, 463
PFO-Ir2	385	385	448, 468	442, 616
PFO-Ir12	378	381	468, 618	469, 619
PFO-Ir16	381	380	622	620

the guest iridium(III) complex (see Figure S1 in the Supporting Information), an energy transfer exists for these polymers.

From Figure 1a, we can see that only strong blue emission bands were observed for PFO-Ir2 in solution, which were assigned to π–π* transitions of polymer backbones. This assignment is confirmed by observation in PFO without iridium(III) complex. On the other hand, an emission band at 617 nm is observed for PFO-Ir12 and PFO-Ir16. This band is assigned to the emission from iridium(III) complex, the intensity of which is enhanced with an increase in iridium(III) complex content, thereby indicating a more efficient energy-transfer process. However, there is still strong blue emission from polymer host, even for PFO-Ir12, which has high iridium(III) complex content of 12%.

The PL spectra of copolymers in film were also investigated (see Figure 1b). Even at low iridium(III) complex content, there is still strong red emission from iridium(III) complexes, thus indicating more efficient energy transfer in film than in solution.

Compared with those of PFO, it is interesting to observe that the blue emission bands from the host were redshifted. One possible reason for the redshift is the β-phase formation of the polyfluorene backbone,[21] which was confirmed by the PL (Figure 2a) and excitation spectra (Figure 2b) of solutions of PFO-Ir2 in THF with different concentrations. From Figure 2a we can see that the emission bands of PFO-Ir2 in dilute solutions were quite similar to those of PFO solution. These bands were assigned to the emission from the α phase of polyfluorene. With an increase in concentration, the emission bands were redshifted, which were tentatively assigned to the formation of the β phase of the polymer backbone. At a concentration of 10^{-3} M, the emission bands from the α phase disappeared completely and only bands assigned to the β phase were observed. This was also demonstrated by the excitation spectra of solutions of PFO-Ir2 in THF with different concentrations. From Figure 2b we can see that a new band at 440 nm assigned to the β phase was dominated at the concentration of 10^{-3} M, further indicating that almost only the β phase was present at such high concentration. The formation mechanism of the β phase can be assigned to the aggregation of polymer chains with an increase in concentration through octyl chain interaction, which can help the planarization of polymer backbones and lead to the formation of the β phase.

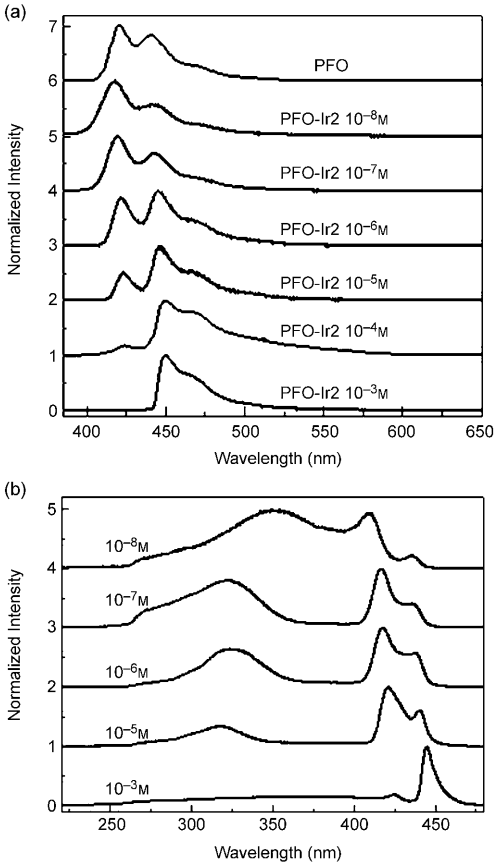

Figure 2. a) PL spectra of solutions of PFO-Ir2 in THF with different concentrations and PFO in THF. b) Excitation spectra of solutions of PFO-Ir2 in THF with different concentrations monitored at 490 nm.

Optical response of [Ir(thq)$_2$(dbm)] (thq = 2-(thiophen-2-yl)-quinoline, dbm = dibenzoylmethanate; 4) to mercury(II): Considering that there is a sulfur atom as a mercury-coordinating element in the C^N ligand, the application of [Ir(thq)$_2$(dbm)] (**4**) as a probe for mercury(II) was investigated through UV/Vis absorption and PL spectra. As shown in Figure 3a, the UV/Vis absorption spectra revealed obvious changes after the addition of mercury(II) to the solution of **4** in CH_3CN (20 μM). Complex **4** showed intense absorption bands in the ultraviolet region of 280–400 nm, which were assigned to the spin-allowed singlet ligand-centered (^{1}LC) transitions. In addition, weak absorption bands at 400–550 nm were also observed, which were assigned to the mixed singlet and triplet metal-to-ligand charge transfer (MLCT) and intraligand (LC_{C^N}) π–π* transitions. Upon addition of mercury(II) to the solution of **4**, the absorption band at 518 nm decreased until it disappeared completely, whereas a new band at 440 nm appeared gradually and corresponded to a $\lambda_{max(abs)}$ blueshift of 78 nm, which induced an evident color change from red to yellow (see Figure 4a). Three clear isosbestic points at 468, 412, and 378 nm were observed. The titration curve was given by the variation in $A_{518\,nm}/A_{440\,nm}$ with respect to the equivalents of mercury(II) added. As shown in the inset of Figure 3a, $A_{518\,nm}/A_{440\,nm}$ decreased continuously until about 1.0 equiv of mercury(II) was added. Further addition of mercury(II) induced only

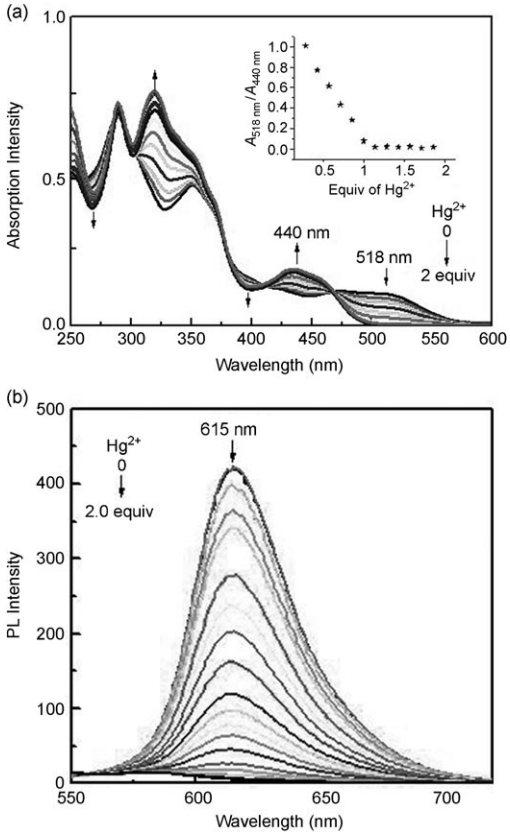

Figure 3. a) UV/Vis absorption and b) PL ($\lambda_{ex}=380$ nm) spectra of a solution **4** in CH_3CN (20 μM) with various amounts of mercury(II). Inset: Titration curve of **4** with mercury(II).

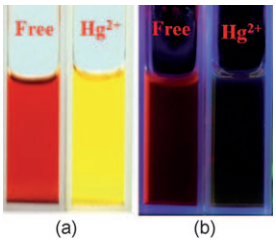

Figure 4. a) Solution and b) emission color observed in air-equilibrated solution of **4** in CH_3CN (20 μM) in the absence and presence of mercury(II) (1.5 equiv).

little changes in $A_{518\,nm}/A_{440\,nm}$, thus implying that **4** forms a 1:1 complex with mercury(II).[12a] Furthermore, the response was fast and a distinct color change of the complex solution could be observed within several seconds. This probe could therefore be used for real-time tracking of mercury(II) with ratiometric and colorimetric detection.

The luminescent response of **4** to mercury(II) was also investigated as shown in Figure 3b. A solution of **4** in CH_3CN (20 μM) exhibited an intense emission band at 615 nm. Upon addition of mercury(II), the emission peak at 615 nm decreased gradually and was quenched finally, thereby realizing naked-eye detection (see Figure 4b). Notably, an evident fluorescent signal change was observed even when the concentration of mercury(II) was as low as 0.5 ppm (see Figure S2a in the Supporting Information).

Optical response of conjugated polymers to mercury(II): Given the significant influence of mercury(II) on the optical properties of complex **4**, we investigated the sensing ability of conjugated polymers (PFO-Ir12 as an example). Figure 5 shows the absorption response of a solution of PFO-Ir12 in THF (20 μM) to mercury(II). With an increase in the amount of mercury(II), the absorbance at 378 nm decreased and that at 418 nm increased with three clear isosbestic points at 444, 400, and 340 nm, thereby resulting in the solution color change from orange to yellow and consequently realizing naked-eye detection (see Figure 5, inset).

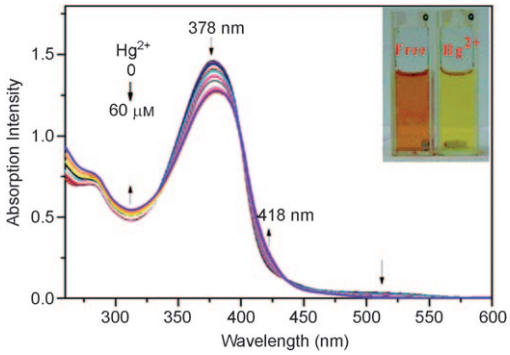

Figure 5. UV/Vis absorption spectra of a solution of PFO-Ir12 in THF (20 μM) with various amounts of mercury(II) ions (0–60 μM). Inset: solution color of PFO-Ir12 in THF (20 μM) in the absence and presence of mercury(II).

Figure 6a shows the luminescent response of PFO-Ir12 to mercury(II). Upon addition of mercury(II), the emission peak from iridium(III) complex at 618 nm decreased until it was quenched completely, which is similar to complex **4**. Unexpectedly, the emission peak at around 460 nm assigned to the polymer main chain was enhanced and was redshifted to 509 nm simultaneously. And a distinct emission color change from red to yellow-green (Figure 6a, inset) was observed, thereby realizing the ratiometric and naked-eye detection toward mercury(II). The response was fairly fast, and we could observe a distinct color change within several seconds. Moreover, the titration curve of a solution of PFO-Ir12 in THF (200 μM) with mercury(II) was given by the variation in $I_{618\,nm}/I_{509\,nm}$ ($I_{618\,nm}$ and $I_{509\,nm}$ represent emission intensities at 618 and 509 nm, respectively) with respect to the concentration of mercury(II). $I_{618\,nm}/I_{509\,nm}$ decreased continuously and reached a saturated point when the concentration of mercury(II) was 40 μM (Figure 6b). Also, the ratio of emission intensities at 618 and 509 nm exhibits a dramatic change from 3.44 to 0.029. Such a large change in emission intensity ratios at two wavelengths is desirable for ratiometric probes, because the sensitivity as well as the dynamic range of ratiometric probes are controlled by the emission ratio. Furthermore, the difference in emission wavelength between host and guest is very large (109 nm). This difference not only contributes to the accurate measurement of the intensities of the host and guest emission peaks, but also

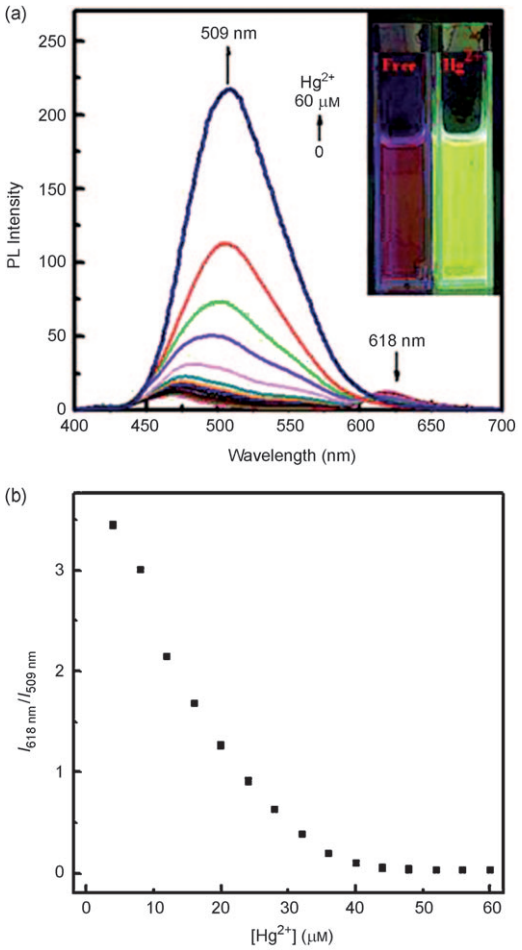

Figure 6. Changes in the PL spectra of a solution of PFO-Ir12 in THF with various amounts of mercury(II) ions (0–60 μM). Inset: a) emission color of a solution of PFO-Ir12 in THF (200 μM) in the absence and presence of mercury(II) and b) titration curve of PFO-Ir12 with mercury(II) (0–60 μM).

results in a huge ratiometric value. More importantly, $I_{618\,nm}/I_{509\,nm}$ changed almost linearly with the concentration of mercury(II) in the range of 0–40 μM, as shown in Figure 6b, thus indicating that the copolymers could also be suitable for mercury(II) monitoring and quantification at 0–40 μM. Besides, both the absorption and luminescent responses of polymer PFO-Ir16 to mercury(II) were investigated as shown in Figures S3–S5 of the Supporting Information. The results were similar to those of PFO-Ir12.

Sensitivity is very important for a chemical probe.[22] Therefore, some experiments were made to investigate the sensitivity of this class of conjugated polymer probes. We gradually decreased the concentration of mercury(II) and measured the PL spectra, respectively. A pronounced fluorescent signal change was still observed even when the concentration of mercury(II) was as low as 5×10^{-10} M, which corresponds to 0.5 ppb (Figure S2b in the Supporting Information). This means that the real limit of detection (LOD, which was calculated as three times the standard deviation of the background noise[2a]) of PFO-Ir12 is lower than 0.5 ppb, which is also significantly lower than that of complex **4**. Hence, PFO-Ir12 exhibits amplified signal outputs with high detection sensitivity due to the effect of the "molecular wires" of conjugated polymer. More significantly, the detection sensitivity of PFO-Ir12 is even lower than the upper limit of 2 ppb that United States Environmental Protection Agency (EPA) mandated for mercury(II) in drinking water,[23] thus showing the prospect of practical applications in toxicology and environmental sciences.

For an excellent probe, high selectivity is a matter of necessity. To study the selectivity of our polymer probe to mercury(II), the absorption responses of a solution of PFO-Ir12 in THF (20 μM) to other twelve different metal ions such as sodium(I), potassium(I), magnesium(II), silver(I), nickel(II), cobalt(II), iron(III), copper(II), lead(II), cadmium(II), chromium(II), and zinc(II) were also investigated. For other metal ions except mercury(II), there was little change in the absorption spectra upon the addition of these metal ions, probably due to the poor coordination ability of the polymer with these metal ions. However, evident variations in absorption spectra were observed after addition of mercury(II) to the solution that contained other cations (see the absorption spectra in Figures S6 and S7 of the Supporting Information). From Figure 7, we can see clearly that PFO-Ir12 exhibits excellent selectivity and competitive ability for mercury(II) over other cations. Only copper(II) caused a slight change of the absorption intensity due to its similar extranuclear electron configuration to that of mercury(II).

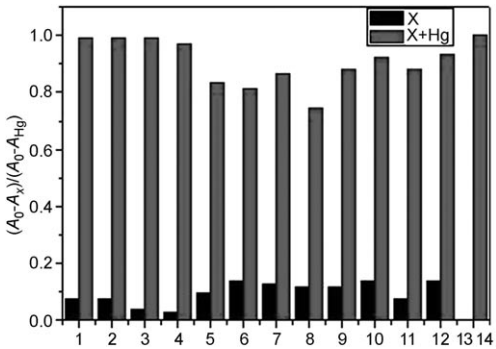

Figure 7. Absorption response of PFO-Ir12 (20 μM) in the presence of various metal cations in THF. Bars represent the absorption intensity ($A_{378\,nm}$) at 378 nm. Black bars represent the addition of various metal cations (60 μM) to the PFO-Ir12 solution; red bars represent $A_{378\,nm}$ after the addition of mercury(II) (60 μM) to the above solutions: 1) sodium(I), 2) potassium(I), 3) magnesium(II), 4) silver(I), 5) nickel(II), 6) cobalt(II), 7) iron(III), 8) copper(II), 9) lead(II), 10) cadmium(II), 11) chromium(II), 12) zinc(II), 13) without metal cations, and 14) mercury(II). A_0 represents the absorbance of blank solution of 20 μM solution of PFO-Ir12 without any metal cation; A_x represents the absorbance after adding various metal cations to the above solution; A_{Hg} represents the absorbance after addition of mercury(II) (60 μM) to the above solutions with different metal cations.

Sensing mechanism: Considering the significant response of complex **4** and conjugated polymers to mercury(II), it is very important to investigate the sensing mechanism, which

will be helpful to the further design of such a class of novel sensing materials. Hence, to clarify the sensing mechanism, several other experiments were carried out.

First, the response of PL spectrum for a solution of PFO in THF to mercury(II) was investigated. No obvious change was observed (Figure S8 in the Supporting Information), thereby implying that host PFO can not respond to mercury(II). Next, the binding process of **4** as a model complex with mercury(II) was investigated in detail. The titration experiment was made for **4** in mixed dimethyl sulfoxide (DMSO) and 4-(2-hydroxyethyl)-1-piperazineethanesulfonic acid (HEPES) buffer solution (DMSO/HEPES = 2:8 v/v) (Figure S9 in the Supporting Information). From the PL spectra, we can see that the emission peak at 621 nm decreased evidently upon addition of mercury(II), thereby indicating that the probe can realize excellent detection even in HEPES buffer solution. Then, saturated ethylene diamine tetraacetic acid (EDTA) aqueous solution, as a metal cation chelator, was added and no evident change in the PL spectra was observed. This indicated that the binding process was irreversible (Figure S10 in the Supporting Information).

To further elucidate the binding mechanism, ^{1}H NMR spectroscopic titration experiments of complex **4** with different equivalents of mercury(II) were conducted. An obvious variation in the ^{1}H NMR spectra of **4** after the addition of mercury(II) was observed (see Figure 8). The characteristic peaks that correspond to free dbm at $\delta = 6.89$, 7.50, and 8.02 ppm appeared upon the addition of mercury(II) and their intensity increased gradually with the continuous addition of mercury(II). Hence, we think that the rupture of Ir–O coordinated bonds occurs and free dbm ligand is released from the complex after addition of mercury(II). From thin-layer chromatography (TLC) of a solution of **4** after the addition of mercury(II), we can observe a new dot assigned to free dbm ligand, which was another piece of evidence to support the decomposition of **4** after binding with mercury(II). From the ESI-MS of complex [Ir(thq)$_2$dbm] (**4**) with mercury(II) (Figure S11 in the Supporting Information), we can observe the peak of m/z at 694.0 that corresponds to [Ir(thq)$_2$(CH$_3$CN)$_2$]$^+$. Furthermore, we synthesized complex [Ir(thq)$_2$(CH$_3$CN)$_2$]OTf and found that its chemical shifts can be found in the ^{1}H NMR spectra of the mixture of **4** with mercury(II).

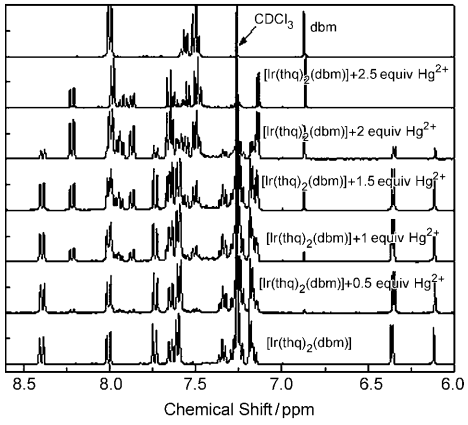

Figure 8. Variation in the ^{1}H NMR spectra of **4** in CDCl$_3$ in the presence of mercury(II) (0–2.5 equiv).

Hence, we tentatively summarize the sensing mechanism of **4** with mercury(II) as follows (Scheme 3a): the sulfur atoms (soft base) on the thq ligand coordinate with mercury(II) (soft acid) according to Pearson's soft and hard acids and bases theory.[24] This kind of interaction between sulfur atoms and mercury(II) has been demonstrated in ruthenium(II) complexes by Palomares et al.[25] The coordination of mercury(II) induces the fast decomposition of **4** with the departure of mercury(II) from the complex to form [Ir(thq)$_2$(CH$_3$CN)$_2$]$^+$ and dbm, which is responsible for the evident spectral variation. According to this mechanism, for polymer PFO-Ir12, the addition of mercury(II) leads to the formation of copolymer PFO-dbm (as shown in Scheme 3b) due to the decomposition of guest iridium(III) complex. For the formed PFO-dbm, fluorene moieties can act as an electron donor and β-diketonate ligand (dbm) moieties as an electron acceptor. The HOMO and LUMO distributions of model compound for PFO-dbm were calculated by DFT. As shown in Figure 9, the HOMO primarily resides on the fluorene moiety and LUMO on the dbm moiety. Hence, an intrachain charge-transfer (ICT) state from fluorene to dbm can be formed in PFO-dbm, thus leading to the significantly enhanced and redshifted emission relative to PFO. Therefore, PFO-Ir12 can act as a polymer chemodosimeter for mercury(II).

Solid-state detection of conjugated polymers for mercury(II): The realization of solid-state detection is quite meaningful for the probe in its practical application in portable sensing devices. The response of polymer PFO-Ir16 film to mercury(II), by way of example, was investigated and is shown in Figure S12 in the Supporting Information. PFO-Ir16 film exhibited an obvious luminescence change after being dipped into the mercury(II) solution in CH$_3$CN for 30 min. The blue emission peak at about 450 nm assigned to the polymer main chain increased, whereas the red emission peak at 618 nm assigned to iridium(III) complexes decreased dramatically, thereby showing that our polymers exhibited excellent sensing performance in the solid state, which will be very useful for the fabrication of sensing devices with fast and convenient detection for mercury(II). To further demonstrate the possibility of such kinds of sensing devices for mercury(II), thin films of PFO-Ir16 were fabricated on silicon gel plates by means of dipping the plate into a solution of PFO-Ir16 in toluene. The patterned film images of the acronym "IAM" (Institute of Advanced Materials) were inscribed by using a writing brush with mercury(II) solution under both visible light and UV light (Figure 10a–d), which showed that the thin film displayed sensitivity to mercury(II). Evident film and emission color changes upon exposure to mercury(II) were observed. Therefore, a sensing device for mercury(II) with excellent performance was realized.

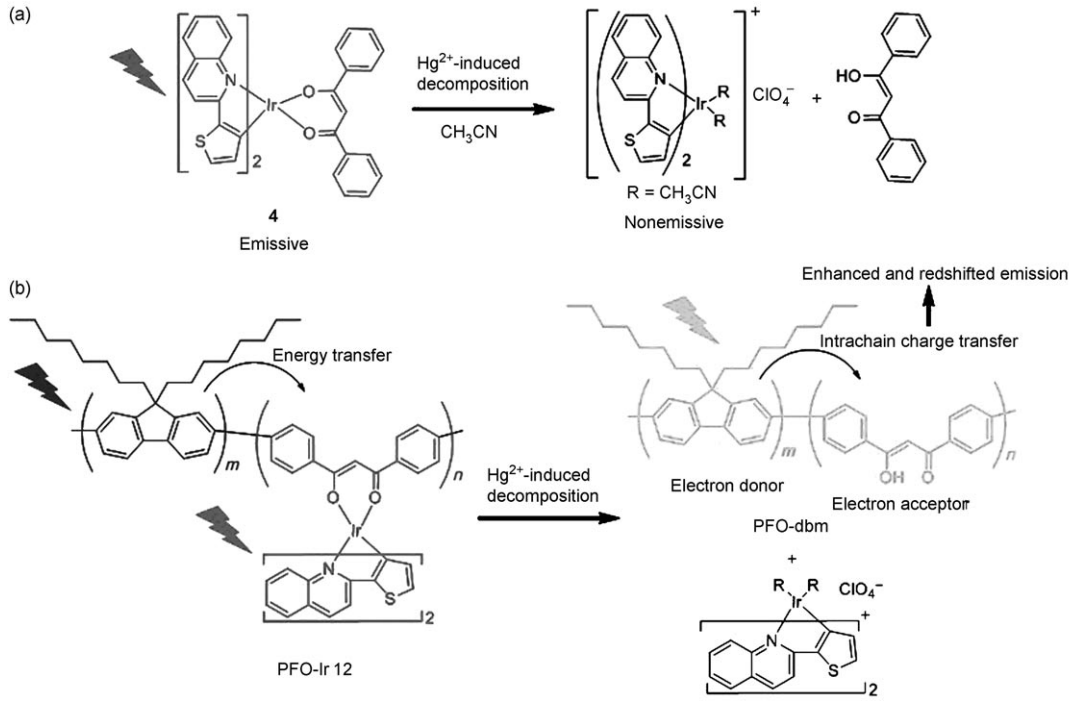

Scheme 3. The illustration of sensing mechanism.

Figure 9. Calculated HOMO (top) and LUMO (bottom) distributions for the model compound of PFO-dbm.

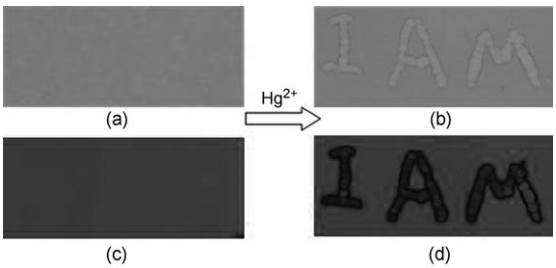

Figure 10. Silicon gel plate coated by PFO-Ir16 under both a) visible light and c) UV light, and the patterned film images of the word "IAM" inscribed by using a writing brush with mercury(II) under both b) visible light and d) UV light.

General design strategies for ratiometric probes based on conjugated polymers that contain phosphorescent heavy-metal complexes: Conjugated polymers that contain phosphorescent heavy-metal complexes have been demonstrated to be a class of very promising optoelectronic materials and have been applied successfully in the field of OLEDs. To realize an alternative application in other fields such as in optical probes is very exciting. Based on our results, we have provided a general design strategy for ratiometric chemosensors or chemodosimeters with switchable phosphorescent and fluorescent signals based on conjugated polymers that contain phosphorescent heavy-metal complexes (see Figure 11). The binding sites or reaction sites for analytes can be introduced into the host or guest. By utilizing the analyte-induced variations in the optical properties of the fluorescent host or phosphorescent guest and subsequent energy transfer from host to guest, the rational design of probes can be realized. Considering the excellent photophysical properties of conjugated polymers and phosphorescent heavy-metal complexes and the rich choice of polymer back-

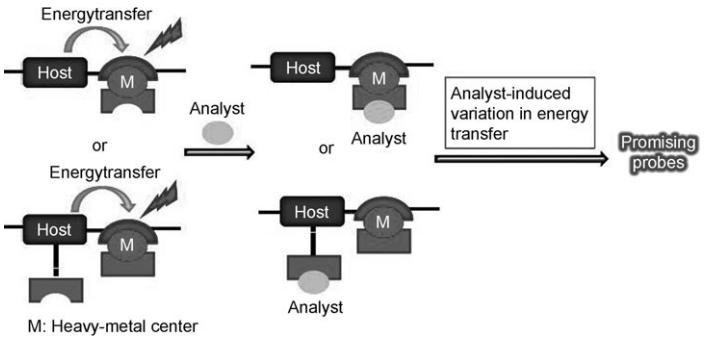

Figure 11. General design strategies for optical probes based on conjugated polymers that contain phosphorescent heavy-metal complexes.

bones and ligands and metal centers of heavy-metal complexes, the application of phosphorescent conjugated polymers as chemosensors or chemodosimeters will be very promising.

Conclusion

In summary, a class of ratiometric chemodosimeters for mercury(II) with high sensitivity and selectivity were successfully realized based on polyfluorenes that contain phosphorescent iridium(III) complexes. The developed polymer chemodosimeters exhibited a dramatic change in the ratios of emission intensities at 618 and 509 nm with switchable phosphorescence and fluorescence. And a remarkable emission color change from red to yellow-green after binding with mercury(II) in THF was observed. The fluorescence response to mercury(II) was not mitigated by other metal cations including sodium(I), potassium(I), magnesium(II), silver(I), nickel(II), cobalt(II), iron(III), copper(II), lead(II), cadmium(II), chromium(II), and zinc(II) were also investigated. The detection sensitivity of this class of polymer chemodosimeters for mercury(II) was as low as 0.5 ppb, which is much lower than the maximal value (1 mg L^{-1}) of mercury(II) concentration in drinking water regulated by the WHO, thereby suggesting the possibility of practical applications in toxicology and environmental sciences. Importantly, the solid films of these polymer chemodosimeters also exhibited high sensitivity and rapid response to mercury(II). The sensing mechanism was assigned to the decomposition of iridium(III) complexes induced by the coordination of mercury(II). As far as we know, this is the first report on chemodosimeters based on conjugated polymers with phosphorescent iridium(III) complexes and this work will be very useful in further extending the application of this class of important light-emitting materials and designing excellent polymer probes.

Experimental Section

Materials: All manipulations involving air-sensitive reagents were performed in an atmosphere of dry N_2 gas. The solvents (THF, toluene and acetonitrile) were purified by routine procedures and distilled under dry N_2 before use. 1,3-Diphenylpropane-1,3-dione, 2-aminobenzaldehyde, 2-ethoxyethanol, 2-acetylthiophene, sodium hydride, 1-(thiophen-2-yl)ethanone, 1-(4-bromophenyl)ethanone, and ethyl 4-bromobenzoate were purchased from Acros. Mercury(II) perchlorate hydrate was obtained from Aldrich. $IrCl_3{\cdot}3H_2O$ was an industrial product and used without further purification. 2-(Thiophen-2-yl)quinoline (thq), iridium–chlorido-bridged dimers, and 1,3-bis(4-bromophenyl)propane-1,3-dione (BrdbmBr) were synthesized according to previous reports.[12b,26]

Measurements: The UV/Vis absorption spectra were recorded using a UV-3600 Shimadzu UV/Vis spectrophotometer. Photoluminescent spectra were measured using an RF-5301PC spectrofluorophotometer. NMR spectra were recorded using a Bruker Ultra Shield Plus 400 MHz instrument. Mass spectra were obtained using a Bruker autoflex matrix-assisted laser desorption ionization time-of-flight (MALDI-TOF/TOF) mass spectrometer or LCQ Fleet ESI mass spectrometer. The gel permeation chromatography (GPC) analysis of the polymers was conducted using a Shimadzu 10 Å with THF as the eluent and polystyrene as standard. The data were analyzed by using the software package provided by Shimadzu Instruments.

Metal cation titration of [Ir(thq)$_2$(dbm)] (4) and PFO-Ir12: Spectrophotometric titrations were performed on 20 μM solutions of **4** in CH_3CN for both UV/Vis absorption and PL spectra, and 20 and 200 μM (the iridium(III) complex concentration of PFO-Ir12) solutions of PFO-Ir12 in THF for UV/Vis absorption and fluorescent spectra, respectively. The solution (2.5 mL) was added into a quartz cuvette, then the UV/Vis absorption and PL spectra of samples were recorded upon the addition of aliquots of fresh mercury(II), respectively. Furthermore, eleven other kinds of cations (e.g., sodium(I), potassium(I), magnesium(II), silver(I), nickel(II), cobalt(II), iron(III), copper(II), lead(II), cadmium(II), chromium(II), and zinc(II)) were also investigated) were tested for selectivity using the same methods.

Theoretical calculations: The structure optimization of the model compound of PFO-dbm was performed using density functional theory (DFT) at the B3LYP level. The 6-31G(d) basis set was used to treat all atoms. The contours of the HOMO and LUMO orbitals were plotted.

Synthesis of monomer [Ir(thq)$_2$(BrdbmBr)] (M_3): Monomer M_3 was synthesized according to the previous report.[9a] A mixture of 2-ethoxyethanol and water (3:1 v/v) was added to a flask that contained $IrCl_3{\cdot}3H_2O$ (0.35 g, 1 mmol) and thq (0.53 g, 2.5 mmol). The mixture was heated at reflux for 24 h. After cooling, the red solid precipitate was filtered to give crude cyclometalated iridium(III)–chlorido-bridged dimer. 2-Ethoxyethanol and BrdbmBr (0.19 g, 0.5 mmol) were added to the mixture of crude chlorido-bridged dimer (0.26 g, 0.2 mmol) and Na_2CO_3 (0.15 g, 1.4 mmol), and then the slurry was heated at reflux for 12 h. After cooling to room temperature, a dark-red precipitate was collected by filtration and chromatographed using CH_2Cl_2/petroleum ether (1:1 v/v) to give M_3 as a red solid. The solid was purified by recrystallization from CH_2Cl_2 and hexane to provide red needlelike crystals (55%, 0.296 g). ^{1}H NMR (400 MHz, $CDCl_3$): δ = 8.29 (d, J = 9.2 Hz, 2H; Ar H), 8.01 (d, J = 8.4 Hz, 2H; Ar H), 7.73 (d, J = 8.4 Hz, 2H; Ar H), 7.65 (d, J = 6.8 Hz, 2H; Ar H), 7.48–7.45 (m, 6H; Ar H), 7.38–7.29 (m, 8H; Ar H) 6.35 (d, J = 4.8 Hz, 2H; Ar H), 6.00 ppm (s, 1H; CH); ^{13}C NMR (100 MHz, $CDCl_3$): δ = 116.66, 124.72, 125.66, 126.70, 127.93, 128.29, 128.95, 129.04, 130.83, 131.25, 134.52. 139.35, 139.76, 150.09, 152.73, 166.81, 178.65, 179.11, 180.67 ppm; MS (MALDI-TOF): m/z: 994.5 $[M+H]^+$.

Synthesis of model complex 4: The synthesis route of **4** was similar to that of M_3. Yield: 46%. ^{1}H NMR (400 MHz, $CDCl_3$): δ = 8.40 (d, J = 8.8 Hz, 2H; Ar H), 8.00 (d, J = 8.8 Hz, 2H; Ar H), 7.74 (d, J = 8.8 Hz, 2H; Ar H), 7.66–7.60 (m, 4H; Ar H), 7.37–7.28 (m, 6H; Ar H), 7.25–7.15 (m, 8H; Ar H), 6.36 (d, J = 4.4 Hz, 2H; Ar H), 6.12 ppm (s, 1H; CH); ^{13}C NMR (100 MHz, $CDCl_3$): δ = 116.66, 124.65, 125.00, 125.67, 126.72, 128.01, 128.71, 128.87, 129.94, 130.65, 134.56, 135.06, 137.32, 138.52, 139.83, 140.81, 150.17, 166.90, 180.24 ppm; MS (MALDI-TOF): m/z: 836.2 $[M+H]^+$.

Synthesis of complex [Ir(thq)$_2$(CH$_3$CN)$_2$]OTf: The complex $[Ir(thq)_2(CH_3CN)_2]OTf$ was synthesized according to the previous reports.[27] Yield: 69%. ^{1}H NMR (400 MHz, $CDCl_3$): δ = 8.75 (d, J = 8 Hz, 2H; Ar H), 8.19 (d, J = 8.4 Hz, 2H; Ar H), 7.84 (m, 4H; Ar H), 7.65 (m, 4H; Ar H), 7.13 (d, J = 4.8 Hz, 2H; Ar H), 2.37 ppm (s, 6H; CH_3); MS (MALDI-TOF): m/z: 694.0 $[M+H]^+$.

Synthesis of conjugated polymers: A small amount of tetrabutylammonium bromide as phase-transfer catalyzer and $[Pd(PPh_3)_4]$ (2.0 mol%) as main catalyst in a degassed mixture of toluene ([monomer] = 0.25 M) and aqueous 2 M potassium carbonate (3:2 v/v) were added to a mixture of M_1 (1 equiv) and dibromo compound (1 equiv), including 2,7-dibromo-9,9-dioctylfluorene (M_2) and Ir complex monomer M_3. The mixture was vigorously stirred at 85–90 °C for 72 h and then bromobenzene was added. After the mixture was cooled to room temperature, it was washed with water. The combined organic phase was concentrated and then it was slowly added dropwise to a mixture of methanol and deionized water (220 mL, 10:1 v/v). A fibrous red solid appeared and was obtained by filtration. The solid was dissolved in THF and then the solution was evaporated. The concentrated solution obtained was dropped slowly into methanol (250 mL) again. This procedure was repeated twice. The fi-

brous solid was filtered and was then washed with acetone in a Soxhlet apparatus for 5 d. The resulting polymers were collected and dried under vacuum. Yields: 44–65 %.

Poly(9,9-dioctylfluorene) (PFO): Yield: 52 %. ^{1}H NMR (400 MHz, $CDCl_3$): δ = 7.68–7.86 (m, 6H; Ar H), 2.11–2.16 (m, 4H; CH_2), 1.14–1.25 (m, 20H; CH_2), 0.79–0.83 ppm (m, 10H; CH_3 and CH_2); ^{13}C NMR (100 MHz, $CDCl_3$): δ = 151.81, 140.68, 140.02, 126.18, 121.49, 120.22, 55.34, 40.43, 31.93, 30.88, 30.08, 29.37, 24.12, 22.64, 14.28 ppm.

PFO-Ir2: Yield: 64 %. ^{1}H NMR (400 MHz,$CDCl_3$): δ = 7.68–7.83 (m, 6H; Ar H of flourene), 2.12 (m, 4H; CH_2 of flourene), 1.14–1.26 (m, 20H; CH_2 of flourene), 0.79–0.85 (m, 10H; CH_3 and CH_2 of flourene), 6.42 (d, 2H; Ar H of Ir complex), 6.28 ppm (s, ×1H; CH of Ir complex); ^{13}C NMR (100 MHz, $CDCl_3$): δ = 151.82, 140.49, 140.05, 126.17, 121.51, 119.97, 55.36, 40.40, 31.80, 30.91, 30.05, 29.23, 23.93, 22.61, 14.07 ppm.

PFO-Ir12: Yield: 65 %. ^{1}H NMR (400 MHz, $CDCl_3$): δ = 7.60–7.83 (m, 6H; Ar H of flourene), 2.12 (m, 4H; CH_2 of flourene), 1.14 (m, 20H; CH_2 of flourene), 0.81 (m, 10H; CH_3 and CH_2 of flourene), 8.48 (d, 2H; Ar H of Ir complex), 8.03 (d, 2H; Ar H of Ir complex), 6.42 (d, 2H; Ar H of Ir complex), 6.28 ppm (s, % ×1H; CH of Ir complex); ^{13}C NMR (100 MHz, $CDCl_3$): δ = 151.82, 140.53, 140.04, 128.78, 127.21, 126.17, 121.51, 119.97, 55.36, 40.41, 31.80, 30.91, 30.05, 29.23, 23.94, 22.61, 14.07 ppm.

PFO-Ir16: Yield: 44 %. ^{1}H NMR (400 MHz, $CDCl_3$): δ = 7.50–7.85 (m, 6H; Ar H of flourene), 2.12 (m, 4H; CH_2 of flourene) 1.14 (m, 20H; CH_2 of flourene), 0.82 (m, 10H; CH_3 and CH_2 of flourene), 8.49 (d, 2H; Ar H of Ir complex), 8.04 (d, 2H; Ar H of Ir complex), 6.43 (d, 2H; Ar H of Ir complex), 6.28 ppm (s, 1H; CH of Ir complex); ^{13}C NMR (100 MHz, $CDCl_3$): δ = 151.82, 140.52, 140.04, 127.31, 126.76, 126.17, 121.51, 119.96, 55.35, 40.40, 31.80, 30.04, 29.71, 29.22, 23.92, 22.61, 14.07 ppm.

Acknowledgements

This work was financially supported by the National Basic Research Program of China (973 Program, 2009CB930601), the National Natural Science Foundation of China (project nos. 50803028, 20804019, and 20774043), the Natural Science Foundation of Jiangsu Province of China (BK2009427), the Natural Science Fund for Colleges and Universities in Jiangsu Province (08KJD430017), the Scientific and Technological Activities for Returned Personnel in Nanjing City (NJ209001), and the Nanjing University of Posts and Telecommunications (project no. NY208045).

[1] Regulatory Impact Analysis of the Clean Air Mercury Rule EPS, U.S. EPA-452/R-05-003, **2005**.

[2] a) M. H. Ha-Thi, M. Penhoat, V. Michelet, I. Leray, *Org. Lett.* **2007**, *9*, 1133–1136; b) M. H. Ha-Thi, M. Penhoat, V. Michelet, I. Leray, *Org. Biomol. Chem.* **2009**, *7*, 1665–1673; c) W. M. Liu, L. W. Xu, H. Y. Zhang, J. J. You, X. L. Zhang, R. L. Sheng, H. P. Li, S. K. Wu, P. F. Wang, *Org. Biomol. Chem.* **2009**, *7*, 660–664.

[3] N. Wanichacheva, M. Siriprumpoonthum, A. Kamkaew, K. Grudpan, *Tetrahedron Lett.* **2009**, *50*, 1783–1786.

[4] E. M. Nolan, S. J. Lippard, *Chem. Rev.* **2008**, *108*, 3443–3480.

[5] *Guidelines for Drinking-Water Quality*, 3rd ed., World Health Organization, Geneva, **2004**, p 188.

[6] D. J. Cho, J. L. Sessler, *Chem. Soc. Rev.* **2009**, *38*, 1647–1662.

[7] C. H. Huang, F. Y. Li, W. Huang, *Introduction to Organic Light-Emitting Materials and Devices*, Fudan University Press, Shanghai, **2005**.

[8] a) W. S. Huang, J. T. Lin, C. H. Chen, Y. T. Tao, S. S. Sun, Y. S. Wen, *Chem. Mater.* **2004**, *16*, 2480–2488; b) M. S. Lowry, S. Bernhard, *Chem. Eur. J.* **2006**, *12*, 7970–7977.

[9] a) S. Lamansky, P. Djurovich, D. Murphy, F. Abdel-Razzaq, H. E. Lee, C. Adachi, P. E. Burrows, S. R. Forrest, M. E. Thompson, *J. Am. Chem. Soc.* **2001**, *123*, 4304–4312; b) W. Y. Wong, G. J. Zhou, X. M. Yu, H. S. Kwok, B. Z. Tang, *Adv. Funct. Mater.* **2006**, *16*, 838–846; c) Y. Chi, P. T. Chou, *Chem. Soc. Rev.* **2010**, *39*, 638–655; d) Q. Zhao, S. J. Liu, W. Huang, *Macromol. Rapid Commun.* **2010**, *31*, 794–807.

[10] a) K. K. Lo, J. S. Chan, L. H. Lui, C. K. Chung, *Organometallics* **2004**, *23*, 3108–3116; b) K. Y. Zhang, K. K. Lo, *Inorg. Chem.* **2009**, *48*, 6011–6025; c) K. K. Lo, K. Y. Zhang, C. K. Chung, K. Y. Kwok, *Chem. Eur. J.* **2007**, *13*, 7110–7120; d) M. X. Yu, Q. Zhao, L. X. Shi, F. Y. Li, Z. G. Zhou, H. Yang, T. Yi, C. H. Huang, *Chem. Commun.* **2008**, 2115–2117; e) Q. Zhao, M. X. Yu, L. X. Shi, S. J. Liu, C. Y. Li, M. Shi, Z. G. Zhou, C. H. Huang, F. Y. Li, *Organometallics* **2010**, *29*, 1085–1091.

[11] Q. Zhao, F. Y. Li, C. H. Huang, *Chem. Soc. Rev.* **2010**, 39, 3007–3030.

[12] a) Q. Zhao, T. Y. Cao, F. Y. Li, X. H. Li, H. Jing, T. Yi, C. H. Huang, *Organometallics* **2007**, *26*, 2077–2081; b) Q. Zhao, S. J. Liu, F. Y. Li, T. Yi, C. H. Huang, *Dalton Trans.* **2008**, 3836–3840; c) Q. Zhao, S. J. Liu, M. Shi, F. Li, H. Jing, T. Yi, C. H. Huang, *Organometallics* **2007**, *26*, 5922–5930; d) Q. Zhao, F. Y. Li, S. J. Liu, M. X. Yu, Z. Q. Liu, T. Yi, C. H. Huang, *Inorg. Chem.* **2008**, *47*, 9256–9264; e) H. L. Chen, Q. Zhao, Y. B. Wu, F. Y. Li, H. Yang, T. Yi, C. H. Huang, *Inorg. Chem.* **2007**, *46*, 11075–11081; f) N. Zhao, Y. H. Wu, H. M. Wen, X. Zhang, Z. N. Chen, *Organometallics* **2009**, *28*, 5603–5611.

[13] a) C. J. Qin, X. F. Wu, B. X. Gao, H. Tong, L. X. Wang, *Macromolecules* **2009**, *42*, 5427–5429; b) S. J. Liu, C. Fang, Q. Zhao, Q. L. Fan, W. Huang, *Macromol. Rapid Commun.* **2008**, *29*, 1212–1215.

[14] a) J. C. Sanchez, A. G. DiPasquale, A. L. Rheingold, W. C. Trogler, *Chem. Mater.* **2007**, *19*, 6459–6470; b) A. Chen, H. S. Sun, A. Pyayt, X. Q. Zhang, J. D. Luo, A. Jen, P. A. Sullivan, S. Elangovan, L. R. Dalton, R. Dinu, D. L. Jin, D. Y. Huang, *J. Phy. Chem. C* **2008**, *112*, 8072–8078.

[15] a) O. R. Miranda, C. C. You, R. Phillips, I. B. Kim, P. S. Ghosh, U. H. Bunzk, V. M. Rotello, *J. Am. Chem. Soc.* **2007**, *129*, 9856–9857; b) B. Liu, G. C. Bazan, *Chem. Mater.* **2004**, *16*, 4467–4476.

[16] a) Y. Chen, Q. L. Fan, P. Wang, B. Zhang, Y. Q. Huang, G. W. Zhang, X. M. Lu, H. S. Chan, W. Huang, *Polymer* **2006**, *47*, 5228–5234; b) D. T. McQuade, A. E. Pullen, T. M. Swager, *Chem. Rev.* **2000**, *100*, 2537–2574.

[17] a) S. J. Liu, Q. Zhao, R. F. Chen, Y. Deng, Q. L. Fan, F. Y. Li, L. H. Wang, C. H. Huang, W. Huang, *Chem. Eur. J.* **2006**, *12*, 4351–4361; b) S. J. Liu, Q. Zhao, Y. Deng, Y. J. Xia, J. Lin, Q. L. Fan, L. H. Wang, W. Huang, *J. Phy. Chem. C* **2007**, *111*, 1166–1175; c) S. J. Liu, Q. Zhao, B. X. Mi, W. Huang, *Adv. Polym. Sci.* **2008**, *212*, 125–144.

[18] B. Liu, W. L. Yu, Y. H. Lai, W. Huang, *Macromolecules* **2002**, *35*, 4975–4982.

[19] X. Gong, J. C. Ostrowski, D. Moses, G. C. Bazan, A. J. Heeger, *Adv. Funct. Mater.* **2003**, *13*, 439–444.

[20] M. A. Baldo, S. R. Forrest, *Phys. Rev. B* **2000**, *62*, 10958–10966.

[21] a) F. B. Dias, J. Morgado, A. L. Macanita, F. P. Costa, H. D. Burrows, A. P. Monkman, *Macromolecules* **2006**, *39*, 5854–5864; b) J. Peet, E. Brocker, Y. H. Xu, G. C. Bazan, *Adv. Mater.* **2008**, *20*, 1882–1885.

[22] Y. P. Zou, M. X. Wan, G. Y. Sang, M. F. Ye, Y. F. Li, *Adv. Funct. Mater.* **2008**, *18*, 2724–2732.

[23] Mercury Update: Impact of Fish Advisories, U.S. EPA, EPA-823-F-01–011, Office of Water. Washington, **2001**.

[24] R. G. Pearson, *J. Am. Chem. Soc.* **1963**, *85*, 3533–3539.

[25] E. Coronado, J. R. Galán-Mascarós, C. Martí-Gastaldo, E. Palomares, J. R. Durrant, R. Vilar, M. Gratzel, M. K. Nazeeruddin, *J. Am. Chem. Soc.* **2005**, *127*, 12351–12356.

[26] K. Zhang, Z. Chen, Y. Zou, C. L. Yang, J. G. Qin, Y. Cao, *Organometallics* **2007**, *26*, 3699–3707.

[27] B. Schmid, F. O. Garces, R. J. Watts, *Inorg. Chem.* **1994**, *33*, 9–14.

Received: March 25, 2010
Published online: September 14, 2010

